Electric Propulsion Facility Optimization via Reduced Order Modeling

IEPC-2024-588

Presented at the 38th International Electric Propulsion Conference, Toulouse, France
June 23-28, 2024

Ehsan Taghizadeh*
University of California, Los Angeles, Los Angeles, CA, 90095, USA

Richard A. Obenchain† and Luke K. Franz‡
Oregon State University, Corvallis, OR, 97331, USA

Richard E. Wirz§¶
University of California, Los Angeles, Los Angeles, CA, 90095, USA
Oregon State University, Corvallis, OR, 97331, USA

For the NASA-funded Joint AdvaNced PropUlsion InStitute (JANUS) program, a reduced order model (ROM) based on the angular coefficient (view factor) method was developed to provide a framework for simulating the neutral density in vacuum chambers during ground-based electric propulsion (EP) systems testing. The time complexity of the developed ROM requires runtimes on order of minutes compared to several hours or more needed to run particle-based kinetic numerical methods thus enabling rapid optimization of the vacuum chamber internal structural design to reduce and minimize desired quantities of the interest (QoI). Incoming molecular flux to thruster exit plane, as the QoI of this study, is the main mechanism affecting the life and performance of the thrusters during ground-based testing. To demonstrate the utility of this modeling approach, a first-order optimization of the beam converger spatial configuration shows nearly 30% reduction in flux to thruster, opening the possibility of further reduction via optimizing other chamber internal structural design such as beam dump.

Nomenclature

K_n	= Knudsen number
λ	= mean free path of the gas molecules (m)
l	= characteristic scale of the system (m)
η_m	= mass utilization efficiency
$\dot{m}_b$	= ion beam mass flow rate (mg/s)
$\dot{m}_a$	= anode mass flow rate (mg/s)
$\Gamma_{i,received}$	= flux received by surface i ($1/(\mathrm{m}^2\,\mathrm{s})$)
$\Gamma_{i,emitted}$	= flux emitted from surface i ($1/(\mathrm{m}^2\,\mathrm{s})$)
$\Gamma_{i,adsorbed}$	= flux adsorbed by surface i ($1/(\mathrm{m}^2\,\mathrm{s})$)

*Postdoctoral Scholar, Mechanical and Aerospace Engineering, ehsant@g.ucla.edu
†Graduate student, College of Engineering, obenchar@oregonstate.edu.
‡Graduate OSGC Fellow, College of Engineering, franzlu@oregonstate.edu.
§Adjunct Professor, Mechanical and Aerospace Engineering, wirz@ucla.edu
¶Boeing Professor, Executive Director of Aerospace Research Programs, College of Engineering, richard.wirz@oregonstate.edu

dA_i = differential surface (m)
$\mathbf{n}_i$ = normal vector to surface i
$\mathbf{r}$ = unit vector from dA_i to dA_j
α_i = sticking coefficient of surface i
P = probability distribution function
v = particle speed (m/s)
m = particle mass (kg)
k_B = Boltzmann constant, 1.38×10^{-23} (J/K)
T = temperature (K)

I. Motivation and Background

The Joint AdvaNced PropUlsion InStitute (JANUS) is a NASA-funded project to investigate the challenges of high-power (∼100 kW) electric propulsion (EP) systems.[1] The mission for JANUS is to predict the in-space lifetime and performance of high-power EP devices via predictive engineering models (PEMs) developed through the probabilistic assessment of ground-based test facility experimental measurements combined with physics-based modeling.[2] The central focus of PEM development is to quantify the impact and uncertainty of facility effects on thruster performance and to extrapolate from in-facility tests to in-space operation.

Vacuum facility design is known to have significant impact on experimental results during ground-based thruster testing.[3] The finite background particle density in a vacuum chamber can modify experimental plume characteristics and therefore the estimated performance of Hall and ion thrusters, obfuscating comparisons to in-space performance; one such important facility effect is interaction of high-energy plume particles with the neutral background particles through charge exchange collisions (CEX).[4] Other particle effects within a ground-based chamber include sputtering of particles from facility surfaces and the transport of those particles back to the thruster face; efforts are more precisely quantifying these sputterants and reducing their presence through the improvement of facility surface design are in progress,[5] but the total particle flux to the thruster is still both non-zero and causes variation in thruster operation both between facilities and between ground-based testing and in-space operation. These inconsistencies may significantly impact mission planning, design, and ultimately realized performance of the EP devices. As such, successful extrapolation from ground to space environments depends on high-fidelity mathematical models that can estimate the neutral and ions density within the vacuum chambers.[6]

This work is aimed to develop a reduced order model (ROM) in order to rapidly simulate the neutral density profile in vacuum chambers during ground-based EP testing. While a vast majority of available models presented in the literature rely on computationally expensive direct simulation Monte-Carlo (DSMC) methods,[7] we demonstrate that the angular coefficient (view factor) method is an indispensable tool to rapidly simulate the three-dimensional (3D) neutral particle transport within the geometrically-complex vacuum chambers used for EP testing. In DSMC methods, the trajectories of randomized particles are computed for solving the Boltzmann equation, generating a result that is inherently subjected to statistical uncertainty. Unlike the DSMC, a ROM based on the angular coefficient method does not require randomization and has significantly reduced computational load when modeling complex geometries and variable boundary value problems. The simulation time for the developed 3D ROM model is on the order of minutes compared with several hours or more needed to run particle tracing codes.

As emphasized in the JANUS vision,[8] the demand for EP thrusters with higher power and consequently increased propellant flow continues to grow. As the primary driver of facility effects, the presence of background neutrals in the chamber escalates with higher propellant flow which in turn influences the ground test results; specifically, the most direct impacts of an increase in facility neutral density are artificial increases in thrust and efficiency through neutral ingestion into the discharge region.[9] Ingestion is based on particle flux to the open surface of the thruster face;[10,11] in simplified analyses, particle flux is generally assumed to be the standard one-sided flux as determined by neutral density near the thruster surface. Standards based on current experimental data have been developed with recommended maximum particle densities for given thruster tests ($\leq 3 \times 10^{-5}$ Torr);[12] to maintain the background pressure below the recommended value while

increasing propellant flow rates, vacuum chambers with enhanced pumping capacity are required. To achieve improved pumping capability, several approaches can be implemented, including: (1) increasing the facility pumping surface, which is often reported as the total additive capability of mechanical and cryogenic pumping systems; (2) improving pumping configuration through strategic placement of the pumps; (3) reducing the conductance losses; and (4) optimizing the chamber internal design.

In this study, we focus on optimizing chamber design as a cost effective approach to reduce the background pressure and, more specifically, molecular flux directed towards the thruster. We particularly define the incoming molecular flux to the thruster exit plane as the objective function of the optimization process due to its prominence in influencing the life and performance of thrusters during ground-based testing.[10] The incoming molecular flux to the thruster contributes to neutral ingestion and charge-exchange ion creation; the former contributing to uncertainty in perceived thruster performance and the latter to electron backstreaming through accelerated grid erosion.[11,13]

The fast ROM model enables optimization of the vacuum chamber internal structural design to reduce and minimize the quantity of interest (QoI), incoming molecular flux to the thruster exit plane, through fast iteration over changes in the design parameters. It is important to note that previously, the design optimization of industrial-scale vacuum chambers was a cumbersome and time-consuming task; our method enables the achievement of these ambitious goals with significantly reduced computational investment. In this work, 2D and 3D ROMs were developed to simulate the neutral density within the Vacuum Test Facility 2 (VTF-2) at the High-Power Electric Propulsion Laboratory (HPEPL) at the Georgia Institute of Technology during operation of an H9 Hall effect thruster. Model parameters were obtained from past experimental results in similar facilities, and experimental ion gauge pressures were used for validation of ROM.

II. Methodology

A. Assumptions

The employed approach is based on the angular coefficient method (described in the next section) with several simplifying assumptions summarized here. First, we assume that many of the dominant processes in EP vacuum facilities are nearly collisionless and therefore can be approximated via view factor modeling; this implies that the Knudsen number is significantly greater than one and that particles collide with chamber surfaces more frequently than each other: $K_n = \lambda/l \gg 1$ where λ is the mean free path of the gas molecules and l is the characteristic scale of the system (chamber).

The second assumption is that the background flow is in thermodynamic equilibrium: cathode and anode mass flow rates as well as all the chamber surface temperatures including the chamber wall and pump surfaces are in steady state. As a result, one can assume that the sticking coefficients of the pumps remain unchanged during the experiment.

The cryosail and cryoshroud temperatures were monitored during the experiment; regardless of their local positions in chamber, they remained below 20K during measurement collection and operation; therefore, one can assume that all the cryosails have the same sticking coefficient for the entire duration of the experiment.

The next assumption is that both reflection and emission of neutrals from all chamber surfaces including the beam target plates are completely diffuse scattering, where particles take on a new velocity characterized by the temperature of the wall. This is often referred to as total accommodation assumption. Specular and diffuse reflection represent two extreme cases that encompass all real surface reflection conditions. Previous findings show that these two extreme cases produce similar results,[14–16] although the difference between them can be analyzed within the uncertainty quantification framework.[17]

Since all interactions between the thruster plume and background molecules including CEX and sputtered particles are neglected (collisionless assumption), we can assume that the ions flowing from the thruster to the downstream facility surfaces undergo neutralization, thermalization, and reflection (100% diffusely) once they collide with the surfaces. Under this assumption, the downstream facility surfaces are simulated as the primary source of propellant mass entering the vacuum chamber. Other researchers have used similar approaches in their efforts to develop reduced order models.[10,18] It is important to note that the foundation of the 2D and 3D ROMs is based on the two primary sources of the neutral flows into the chamber, one source from the thruster exit plane and the second one from the downstream facility surfaces; the ratio of the mass flux from the thruster exit plane to the mass flux from the downstream facility surfaces depends on the mass utilization efficiency of the thruster that changes with internal plasma properties defined as

$$\eta_m = \frac{\dot{m}_b}{\dot{m}_a} \tag{1}$$

where η_m is the mass utilization efficiency, $\dot{m}_b$ is the ion beam mass flow rate, and $\dot{m}_a$ is the anode mass flow rate. It is reported that the the mass utilization efficiency for the H9 and similar thrusters ranges between 86-90% for 300-900 V.[19,20]

B. Angular Coefficient Theory

In the angular coefficient method, the calculation of neutral density is based on integrating the flux received by a surface from all other surfaces within its line-of-sight. Assuming diffuse and cosine law scattering, the arriving flux at the differential surface j from surface i is given by

$$\Gamma_{j,received} = \int_{A_i} \frac{\Gamma_{i,emitted} \cos(\theta) \cos(\theta')}{\pi r^2} dA_i = -\int_{A_i} \frac{\Gamma_{i,emitted} (\mathbf{n}_i \cdot \mathbf{r})(\mathbf{n}_j \cdot \mathbf{r})}{\pi r^4} dA_i \tag{2}$$

where $\mathbf{r}$ is the vector from dA_i to dA_j, and $\mathbf{n}_i$ is the normal vector to surface i as shown in Fig 1. The sticking coefficient of surface determines the portion of the incoming flux that are adsorbed to the surface

$$\Gamma_{j,adsorbed} = \alpha_j \Gamma_{i,received} \tag{3}$$

hence, the reflected flux from surface j is given by

$$\Gamma_{j,emitted} = (1 - \alpha_j) \Gamma_{i,received} \tag{4}$$

Consequently, the flux density leaving the the surface j is given by[21]

$$\Gamma_{j,received} = -(1 - \alpha_j) \int_{A_i} \frac{\Gamma_{i,emitted} (\mathbf{n}_i \cdot \mathbf{r})(\mathbf{n}_j \cdot \mathbf{r})}{\pi r^4} dA_i \tag{5}$$

The probability distribution of the molecular speed in 3D space is given by

$$P(v) = \left(\frac{m}{k_B T} \right)^2 \frac{v^3}{2} \exp\left(-\frac{m v^2}{2 k_B T} \right) \tag{6}$$

which follows a non-Maxwell distribution.[22–24] A closed system of equations for fluxes to and from each surface is developed and solved simultaneously for each state condition; particle gains and losses from emission surfaces and pumps respectively are includes in the matrix.

A comprehensive review of the angular coefficient method is available in literature.[25] This approach is significantly faster than the DSMC method and is not affected by statistical scatter. Similar approaches have been used in past by other researchers[26–28] to simulate particles transport.

C. Numerical Analyses

Neutral density ROM simulation is implemented using COMSOL Multiphysics® to solve the steady-state balance equations implemented on the representative geometry. A convergence analysis was performed based on Richardson extrapolation following Roache[29] in order to ensure that the numerical results are stable. The grid convergence index (GCI), which provides a bound on the estimated error of the numerically converged solution, was computed for the simulations. The imposed condition was that the GCI to be on the order of 1×10^{-4} or less, indicating a grid-independent solution. Each 3D ROM simulation takes approximately 10 minutes, while 2D ROM simulations take less than 10 seconds on typical desktop computer hardware.

III. Model Hierarchy

The inputs to the ROM are: (1) the total mass flow rate to chamber (anode and cathode flow) which is the primary driver of the chamber background neutral density, (2) facility surface temperature profiles obtained from thermocouples placed in various positions inside chamber, which determines the thermal velocity of particles released from or reflected by surfaces in free molecular flow regime, and (3) thruster plume profile

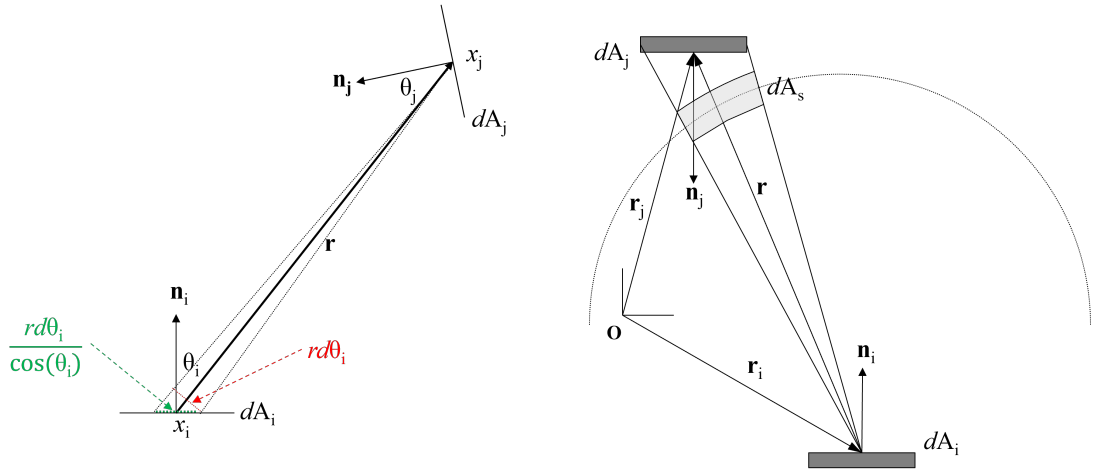

Figure 1: Basics of angular coefficients method shown on two differential surfaces dA_i and dA_j. The flux intensity that arrives on the differential surface j from surface i is given by Eq. (2). Diffuse emission and reflection is assumed.

extrapolated from Faraday probe data which is used to compute the local ion flux from the thruster to downstream facility surfaces. Table 1 summarizes the mass and temperature input parameters to the model. Note that the computed incident particles flux to downstream facility surfaces are used to determine the amount of the neutral particles released from those surfaces in the ROM under the neutralization/thermalization assumption for beam ions. Under this assumption and neglecting the interactions of the plume with the background gas, the amount of the ions incident flux to each downstream facility surface is equal to the amount of neutral released from that surface. Fig 2 shows the ion current density measured in the plume at 300V and 15A for the H9 during testing at HPEPL that was used to compute the incident molecular flux to the downstream facility surfaces. A collective test campaign has been recently completed in VTF-2 as part of the JANUS project.[30] We used the experimental data collected during the test campaign to validate our models.

The outputs produced by the ROMs are incident neutral fluxes and number density profile along with the derived pressure map on the all surfaces.

The sticking coefficient of the pumps is initially inferred by iteratively adjusting the coefficient and comparing the model outputs with the experimental data for the 300V operating condition. Further validation will be performed as additional experimental data is received.

Table 1: The input parameters to the ROM model.

Input Parameter	Value	Unit
Thruster mass flow rate (anode + cathode)	13.6	mg/s
Beam dump tip temperature	120	°C
Beam dump side 1 temperature	75	°C
Beam dump side 2 temperature	70	°C
Thruster body temperature	170	°C
Thruster exit plane temperature	300	°C

IV. Experimental Setup

A. Vacuum Test Facility

The experiments were conducted in VTF-2 at the HPEPL. A schematic of this facility is illustrated in Fig. 4a. The facility is described in detail in previous work.[31] VTF-2 is a stainless-steel chamber with a diameter of

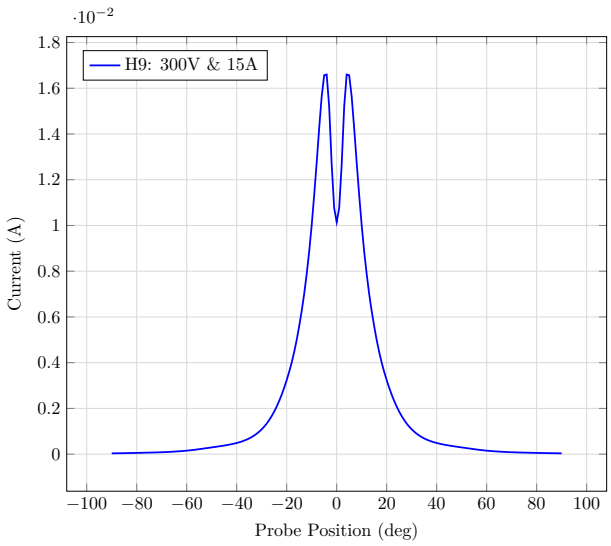

Figure 2: Ion current density measured in the plume at 300V and 15A for H9 during testing at HPEPL.

4.9 m and a length of 9.2 m. High vacuum is achieved by a closed-loop N2 liquefaction system consists of ten CVI TM1200i cryopumps connected to two Stirling cryogenics SPC-4 compressors. The system provides a combined xenon pumping speed of 350 kl/s and achieves a base pressure of 1.9×10^{-9} Torr.

B. Ionization Gauges

The pressure in VTF-2 was monitored using two Agilent Bayard-Alpert (BA) 571 hot-filament ionization gauges controlled by Agilent XGS-600 gauge controllers. The pressure sensitivity range for these ionization gauges is reported to be 1×10^{-3} to 2×10^{-10} Torr. These gauge were configured per the guidelines outlined in the best practices guide for pressure measurement for electric propulsion testing.[12] One ionization gauge is placed 2.45 m radially from the thruster exit plane, referred to as *external* ion gauge. The second ionization gauge is located upstream of the thruster centerline approximately 1 m behind from the thruster, referred as to *internal* gauge. The external ion gauge is perpendicular to the thruster exit plane and is faced towards the thruster, while the internal ion gauge is aligned with the thruster centerline and it is faced away from the thruster. Fig 3 shows the pressure gauges alignment. The reported pressures are corrected for krypton using following relation:

$$P_c = \frac{P_i - P_b}{1.94} + P_b \tag{7}$$

where P_c is the corrected pressure, P_b is the base pressure, P_i is the indicated pressure, and 1.94 is a gas specific correction constant.

C. Hall Effect Thruster

The thruster used in the experiments is the magnetically shielded H9, a 9-kW class Hall thruster developed by the Jet Propulsion Laboratory in collaboration with the University of Michigan and the Air Force Research Laboratory. More information about the H9 can be found in paper by Hofer et al.[32] The centrally mounted lanthanum hexaboride cathode, the anode/gas distributor, and the discharge chamber geometry of the H9 were all inherited from the unshielded 6-kW H6 HET. Total efficiency of the H9 ranges from 61-63% over 300-800V and specific impulse reaches 2950s at 800V, 9kW. In all experiments, neutral krypton atoms flow through the the H9. Mass flow rates and the corresponding pressure measurements from both ionization gauges are reported in Tables 1.

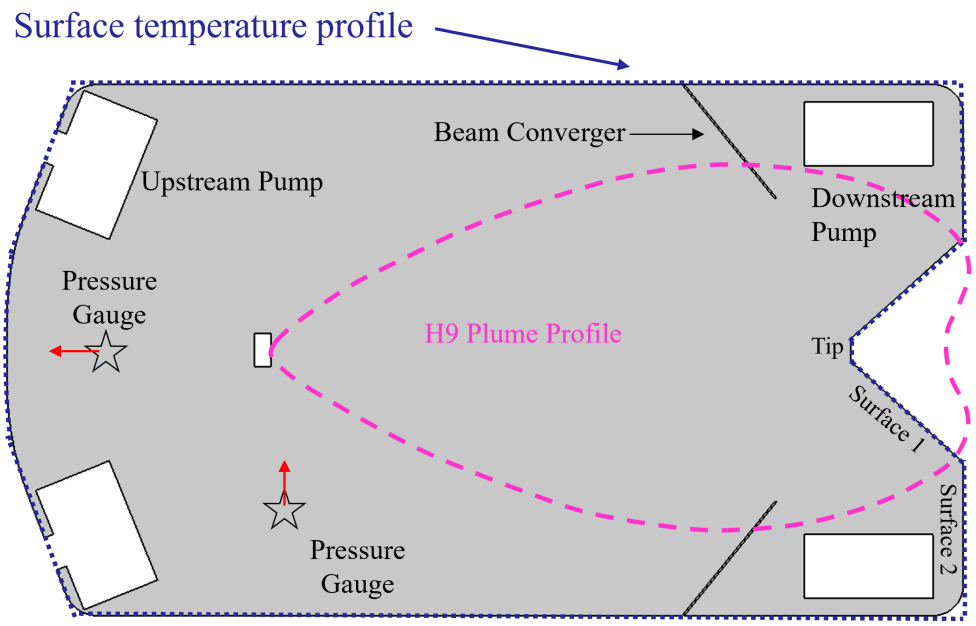

Figure 3: Simplified 2D representation of the VTF-2. This geometry is obtained by the cross section of the 3D VTF-2 computational geometry, Fig 4b, and a horizontal plane crossing the thruster centerline. Two ionization gauge locations are marked with stars, with their orientations indicated by red arrows. The H9 plume profile is illustrated in purple; its computed 3D profile is used for 3D computational domain.

V. Results and Discussion

A. Overview

Several methods can be used to simulate plasma flow, including magnetohydrodynamics, two-fluid models, gyrokinetics, and kinetic methods, listed in order of increasing time complexity of the simulations. Taking into account these assumptions listed in the section A, the reduced order models are developed by releasing the neutrals from different sources into the chamber and then computing the flux and density received by each surface; this approach avoids directly simulating the ion beam, significantly reducing the computational time. It is also worth nothing that the ROMs can be implemented on any vacuum chamber regardless of the geometry and size; for the purpose of this work, we focus on the implementing the model using the HPEPL VTF-2 EP vacuum chamber.

B. 3D Hot Flow ROM

Fig 4a shows the HPEPL VTF-2 EP vacuum chamber and its internal components, which we used to implement the developed reduced order models. Figs 4b and 4c illustrate the simplified 3D computational domain with different highlighted elements. The primary internal features consist of ten cryopumps (4 behind the thruster and 6 surrounding the target), thruster, thruster stand, ionization gauges, beam converger (frustum along the wall near the target), extra converger plates, beam target/dump, and flooring. The floor's grate size is increased while maintaining the porosity of the real chamber grate.

The representative simulated neutral number density distributions for hot flow through the H9 HET are presented in Fig. 5. Several trends are noticeable here: first, Fig 5a illustrates that the neutral density is lowest near the pump regions, which is in accordance with pumps being the only elements in the chamber that can function as particle sinks. Second, neutral density is relatively high between the beam converger and the thruster region; this can be attributed to particle being reflected from the beam converger as well as the beam dump towards this region. Third, the local neutral density in the vicinity of the floor is influenced by the grate as shown in the Fig 5b; this will affect the neutral flux to the thruster exit plane and will be discussed in details in section D. Fourth, the tip of the beam dump has the highest neutral density, which

makes it susceptible to the highest erosion rate.[33,34]

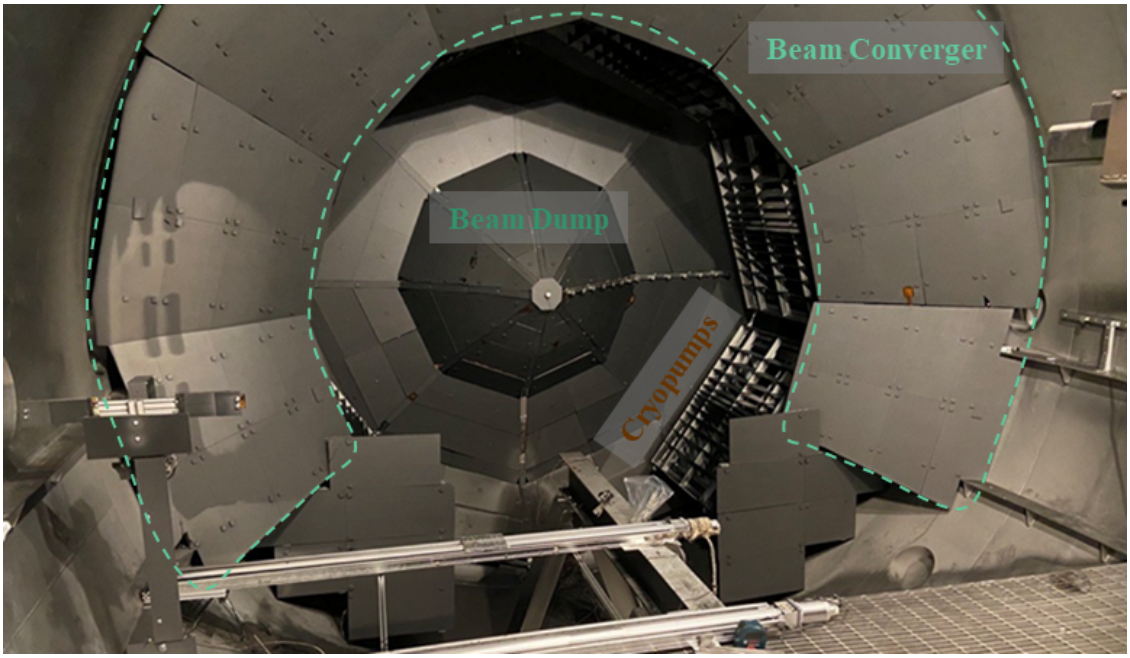

(a)

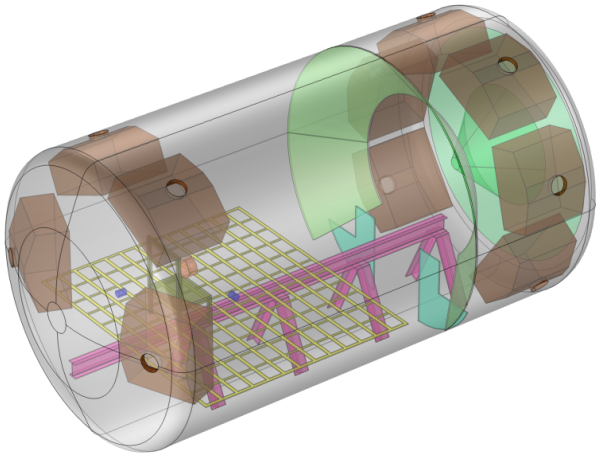

(b)

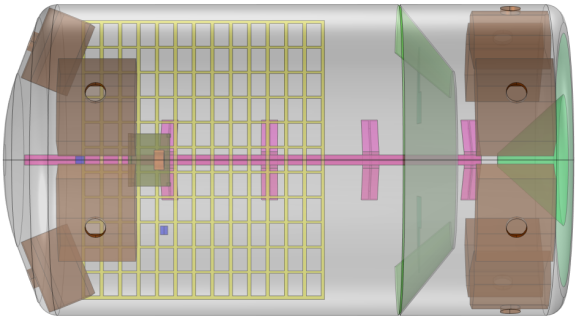

(c)

Figure 4: (a) The interior of the Georgia Tech's High-Power Electric Propulsion Laboratory (HPEPL) VTF-2 vacuum facility equipped with beam converger, beam dump, and ten PHPK-TM1200i cryopumps (not all the pumps are shown here). (b) Simplified 3D computational domain with different highlighted elements: ten cryopumps highlighted in brown, H9 Hall thruster highlighted in orange, two Granville-Phillips 370 hot-cathode Bayard-Alpert ionization gauges highlighted in blue, beam converger highlighted in light green, and beam dump highlighted in green. The floor's grate size is increased while maintaining the porosity of the real one. (c) The top view of the simplified computational domain.

C. 3D Hot Flow ROM Validation through Sticking Coefficient Inference

The 3D ROM was executed for the lower power (300V) operational level in the HPEPL experiment. An initial sticking coefficient of 0.4 (suggested for xenon)[10] was selected based on literature. The model was then iterated through sticking coefficient values until a reasonable approximation (range) of the measured

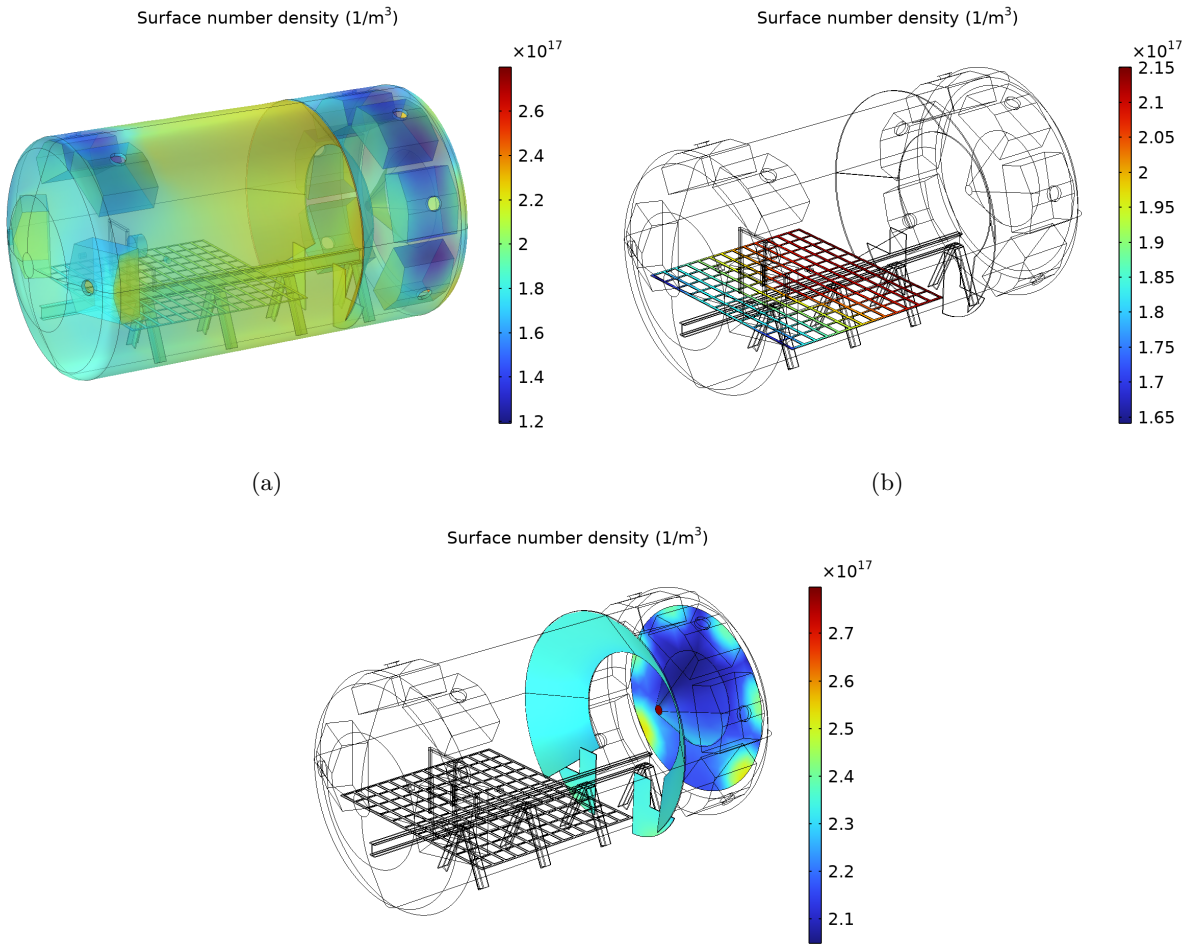

Figure 5: The simulated 3D surface neutral number density distributions for hot flow through the H9 HET for VTF-2 chamber: (a) whole internal surface of chamber, (b) grate, and (c) downstream facility surfaces. The sticking coefficient is 0.3 and mass flow rate is 13.6 mg/s for krypton.

neutral density values was reached. The resulting sticking coefficient of 0.30 remains within experimental expectations.

To validate the model, we then executed the 3D ROM for the high power (600V) operational level and compared the resulting neutral density values to experimental measurements from the same campaign. The results were likewise similar to the initial approximation. Due to the small variance between the initial and validation case, a more robust validation of the model with the current sticking coefficient is planned when additional experimental data is received later in 2024. Table 2 shows the comparison between the experimental pressure data and simulation results for the low power case.

D. Floor Effect

In this section, we have investigated the effects of the floor on the neutral flux to thruster as the objective function of this study. The floor components will decrease the effective volume (empty space) of the chamber which, in turn, increases the neural density and background pressure in the chamber. Furthermore, the flooring acts as a partially transparent surface which can change particle trajectories and act to modify neutral flux directed towards the thruster face, especially as the flooring is below the centerline of the chamber and thus has higher flux from the top than from below.

Table 2: Comparison between the experimental pressure data and simulation results for low power case, 300 V.

	Experiment (Torr)	3D ROM (Torr)
internal ionization gauge	6.0×10^{-6}	6.0×10^{-6}
external ionization gauge	5.4×10^{-6}	5.6×10^{-6}

To quantify this effect, two simulations were executed with identical parameters: one with the flooring present in the standard/default configuration, and one with the flooring being removed. The resulting changes in neutral flux to the thruster face within the chamber can be seen in Fig .6. As shown, the flux to the thruster increases with the presence of the floor in a nonlinear manner; in the case of sticking coefficient of 0.4, the increase in flux to the thruster face by including the floor is approximately 5% over the simulation without the floor, whereas in the sticking coefficient of 0.3 case, the increase is only 3%. This nonlinearity is likely due to particle reflections from the floor's surface towards the thruster rather than changes in the volume of the chamber due to the physical volume of the floor or its segmentation of the chamber.

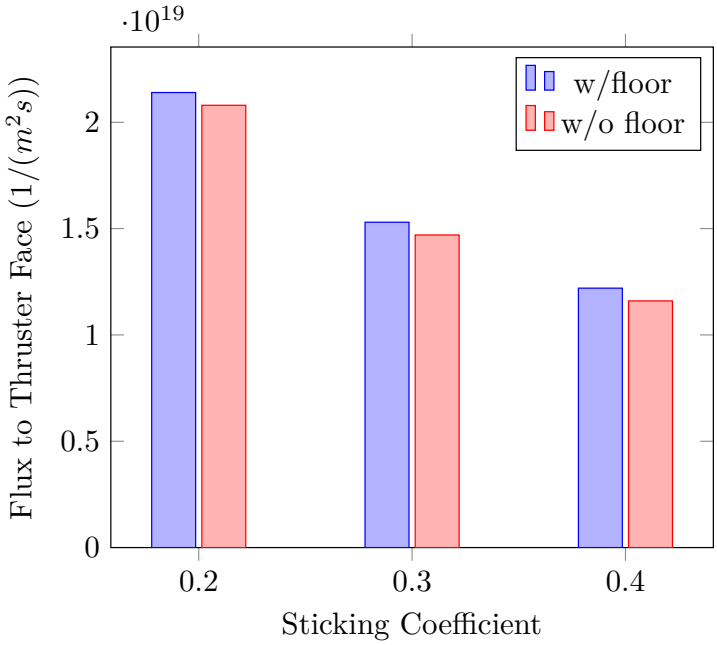

Figure 6: The flux to thruster face as a function of the pumps sticking coefficient for the cases where (1) floor is present in the chamber, and (2) floor is removed.

VI. Optimization

One of the greatest advantages of the developed ROM is the ability to iterate rapidly through multiple design scenarios to target specific design parameters or objective functions. Using this method, we explore how changes in the internal design of the vacuum chambers impact the flux of neutral particles to the thruster face and thus drive facility effects such as ingestion and charge exchange. In order to reduce and ideally minimize the flux to thruster exit plane, we focus on the optimizing the beam converger pivot location (d), its angle to wall (θ), and its length (L') in the 2D representative geometry(Fig. 7a); these three degrees of freedom makes it possible to explore all the possible options that the converger spatial configurations can take. As a first order approach, we perform sweeps of these parameters between practical limits to investigate which combinations best divert the neutrals away from the thruster exit plane.

Since the 2D representative geometry varies in effective pumping area, chamber surface area, and down-

stream facility area from the realistic 3D geometry, results from the 3D simulations are used to drive the 2D model: we adjust the mass flow rate of the 2D model to match the results of flux to thruster in the 3D simulations. In this way, the 3D ROM informs the 2D ROM.

The process for optimization is shown in Fig. 7b: development of the 3D ROM; validation of the 3D ROM against experimental data; using simulation results from the 3D ROM to inform and drive the 2D ROM; and executing the optimization sweeps using the 2D ROM. Once the preliminary optimized geometry is obtained in 2D, those results are used to limit the parameter space and inform the 3D optimization, which will produce the final optimized geometry.

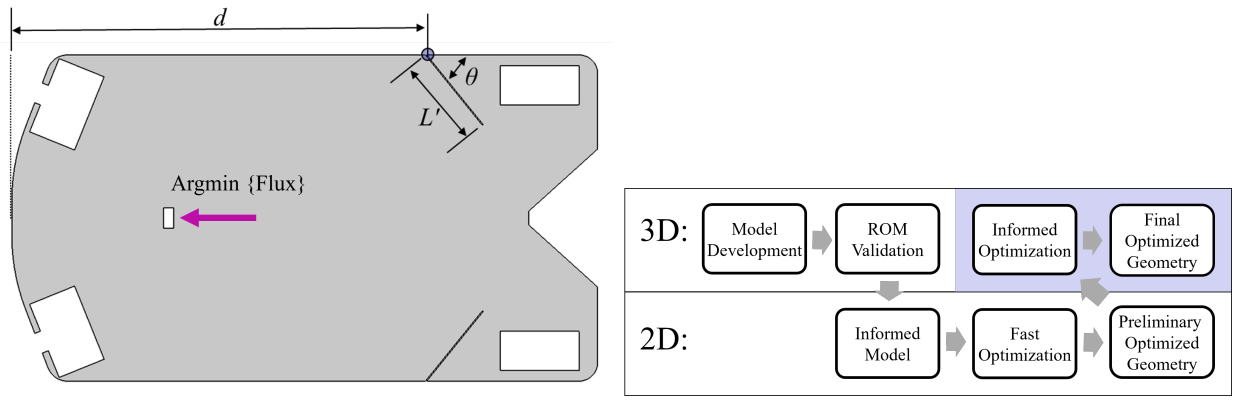

(a) (b)

Figure 7: (a) Three degree of freedoms for optimizing the beam converger: (1) converger pivot location d, its angle to wall (θ), and its length (L'). The purpose of the this optimization is to reduce and minimize flux to thruster exit plane. (b) The optimization framework as follows:(1) 3D ROM model development, (2) 3D ROM model validation, (3) 2D ROM model development informed by validated 3D ROM model, and (4) beam converger optimization.

A sample neutral density profile comparison between two cases with higher and lower flux to thruster is shown in Fig. 8; these cases have the same pivot locations ($d = 7.0$ (m)) and length ($L' = 1.56$ (m)) but varying angles. For the case with higher angle to the wall, the area of the beam target region is enlarged and enables the containment of a larger portion of neutrals, thus trapping them in the downstream facility region to then be pumped away by cryopumps (lower inset). In the lower angle case, the beam target region area is minimized, and more particles escape to the main body of the chamber where they may impact the thruster face (upper inset). For this specific length and pivot location configuration, the flux to the thruster face is seen to be linearly trending with the angle to the chamber wall.

The flux to thruster exit plane as a function of the angle to the chamber wall for four different beam converger pivot locations and lengths are shown in Fig 9. The lowest achieved fluxes to thruster face are shown in the box, and the corresponding neutral density profile are shown in Fig 10. The flux to thruster is determined by balancing two primary particle motions: first, trapping or containing as many particles behind the converger in the region of the target and pumps; second, by reducing the flux of particles reflected off the converger directly back towards the thruster. As shown, the shorter converger lengths reduce flux better at more radial orientations, as they do not impinge upon the ion beam as significantly and therefore "reflect" lower particle counts to the main body of the chamber; in this position, they also trap as many particles in the beam target region as possible. Longer convergers must be angled more sharply and towards the wall to prevent impinging upon the beam; however, they can be shifted further towards the target to compensate for the angular positioning and continue to generate high particle density regions near the target.

As a consequence of the angular coefficient method used for neutral transport, particles are assumed to be traveling based on thermal flux principles. Therefore, minimizing the flux to the thruster face also corresponds to a minimum average chamber neutral density.

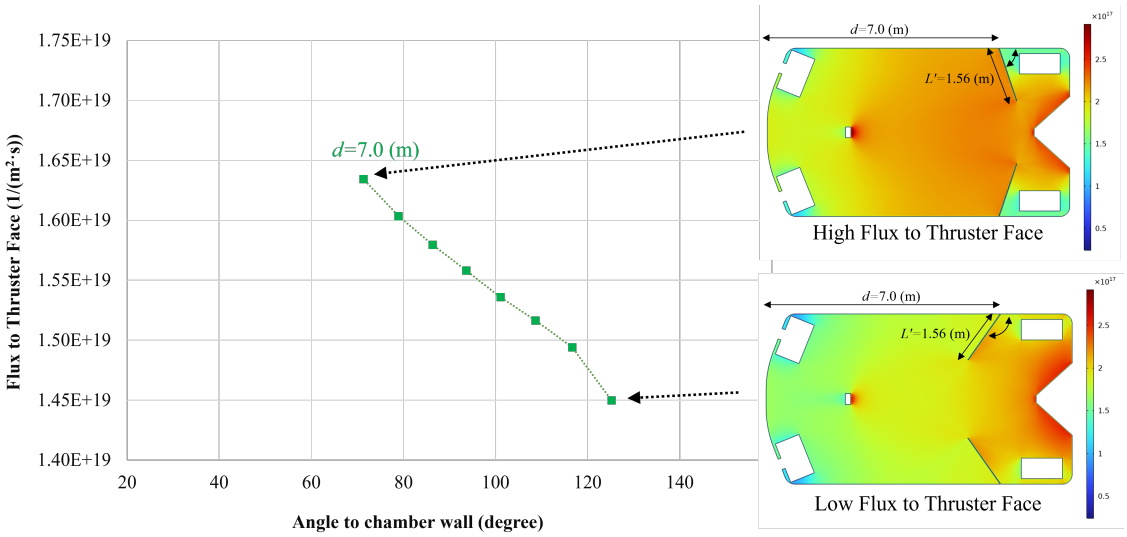

Figure 8: The neutral density profile comparison between cases with highest and lowest flux to thruster; both cases have the same pivot locations ($d = 7.0$ (m)) and length ($L' = 1.56$ (m)).

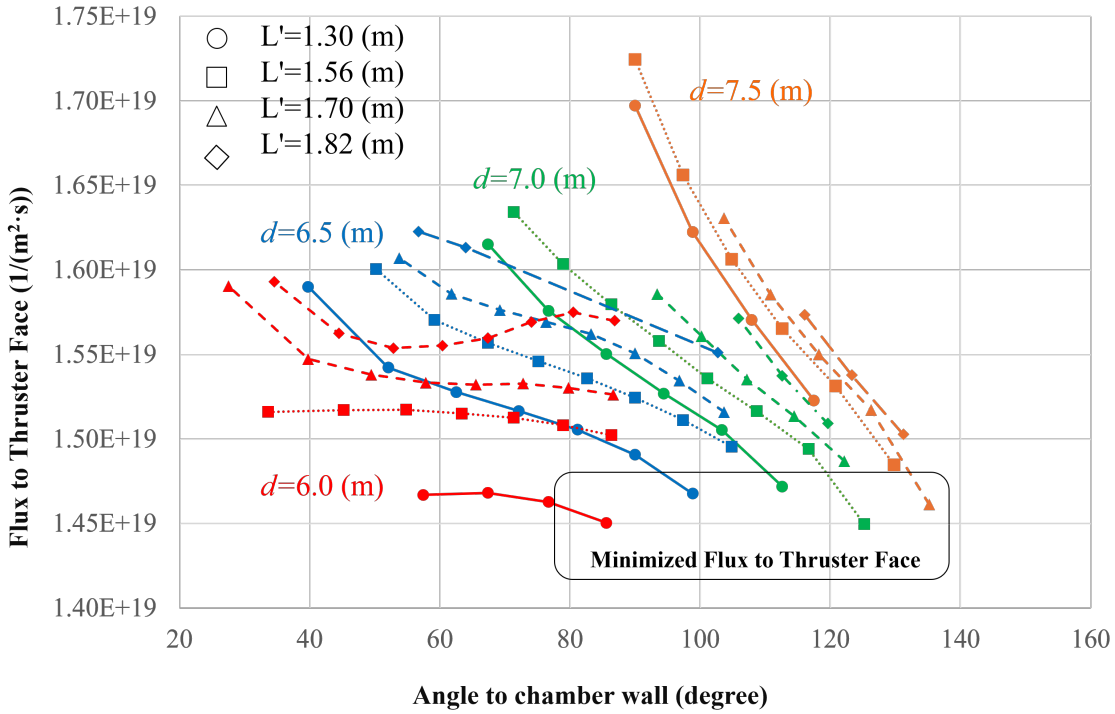

Figure 9: The flux to thruster exit plane a function of the angle to the chamber wall depicted for four different beam converger pivot locations, highlighted in different colors. Different markers show different beam converger length. The lowest achieved fluxes to thruster are shown in the box.

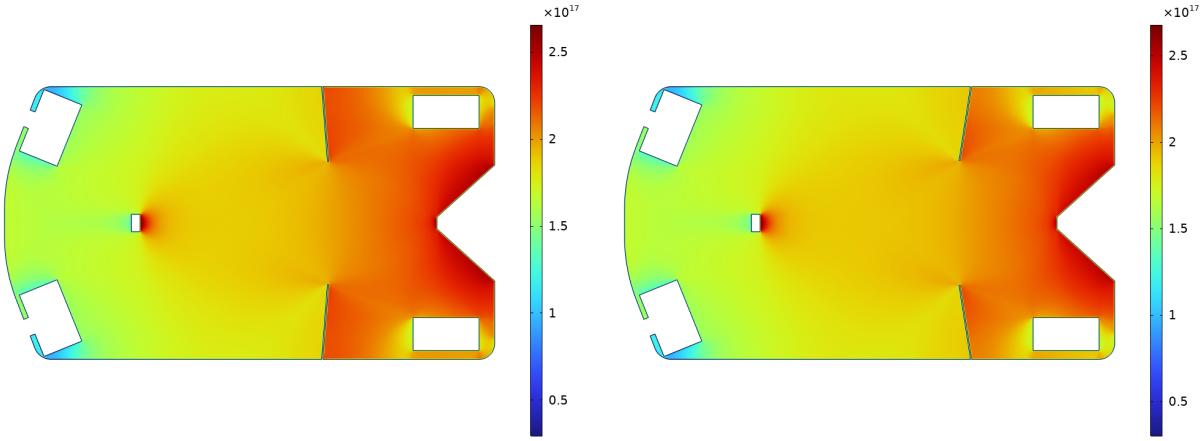

(a) $d = 6.0$ (m)

(b) $d = 6.5$ (m)

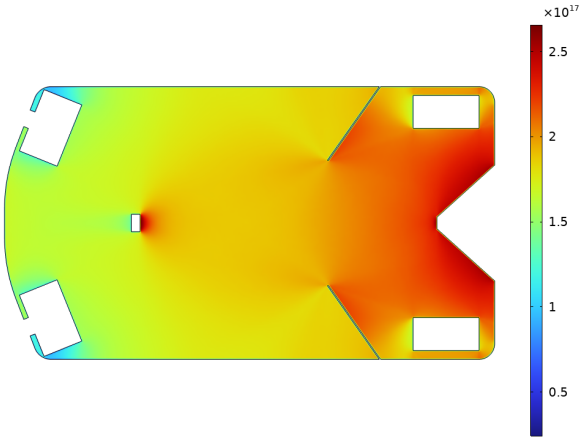

(c) $d = 7.0$ (m)

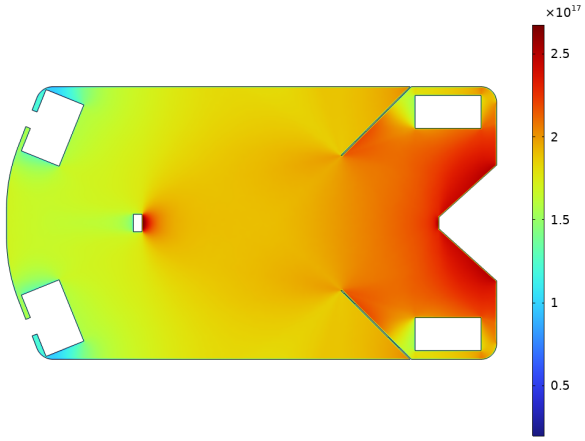

(d) $d = 7.5$ (m)

Figure 10: Neutral density profile for the lowest flux to thruster face for each beam converger pivot location: (a) $d = 6.0$ (m), (b) $d = 6.5$ (m), (c) $d = 7.0$ (m), and (d) $d = 7.5$ (m).

VII. Conclusion

In support of the development of high-powered thrusters as led by the Joint Advanced Propulsion Institute (JANUS) under NASA's guidance, we have developed 3D and 2D reduced order electric propulsion test facility models based on the angular coefficient (or view factor) method. To avoid requiring particle tracking methods for the ion beam, the models are based on neutralization and thermalization of ions upon impact with facility surfaces, allowing these surfaces to act as neutral emission locations and reducing computational overhead for the ROM. More rigorous validation is planned using future experimental data from the ongoing test campaign.

Exploration of the ROM results include analysis of the impact of specific chamber components as well as determining the sticking coefficient for the given test conditions. As an example of component impact, the presence of the grated flooring was shown to increase incoming flux to thruster face by approximately 5-10%. The sticking coefficient for krypton at the 300V/15A operating condition was found to be 0.30. Additionally, optimization of an example test chamber was completed by sweeping specific chamber design parameters to reduce neutral flux to the thruster face. A maximum of 30% reduction in neutral flux to the thruster was shown between potential configurations with four specific cases resulting in similar chamber densities and flux to the thruster, demonstrating the potential benefit of leveraging fast ROMs for facility design and optimization. Future improvements and analysis will continue by using the 2D optimization results to inform the parameter space for more detailed 3D optimization. Finally, these ROMs will be extended to account for sputterants transport.

Acknowledgments

The authors fully acknowledge support from the Joint Advanced Propulsion NASA Space Technology Research Institute. This work was funded by Joint Advanced Propulsion Institute 20-STRI-FULL-0004, NASA Grant Number 80NSSC21K1118.

References

[1]Mitchell LR Walker, Dan Lev, Maryam Saeedifard, Benjamin Jorns, John Foster, Alec D Gallimore, Alex Gorodetsky, Joshua L Rovey, Huck Beng Chew, Deborah Levin, et al. Overview of the joint advanced propulsion institute (janus). In *37th International Electric Propulsion Conference*, pages IEPC–2022–156, 2022.

[2]Richard E Wirz, Alex A Gorodetsky, Benjamin A Jorns, and Mitchell LR Walker. Predictive engineering model for life and performance assessment of high-power electric propulsion systems. In *37th International Electric Propulsion Conference*, pages IEPC–2022–410, 2022.

[3]Richard R Hofer, Peter Y Peterson, and Alec D Gallimore. Characterizing vacuum facility backpressure effects on the performance of a hall thruster. In *Proceedings of the 27th International Electric Propulsion Conference*. IEPC-01-045, 27th International Electric Propulsion Conference, Pasadena, CA, 2001.

[4]Mitchell LR Walker, Alec D Gallimore, Iain D Boyd, and Chunpei Cai. Vacuum chamber pressure maps of a hall thruster cold-flow expansion. *Journal of Propulsion and Power*, 20(6):1127–1132, 2004.

[5]Graeme Sabiston and Richard E. Wirz. Electric propulsion vacuum chamber design approaches for reducing sputtering effects. In *38th International Electric Propulsion Conference*, pages IEPC–2024–187, 2024.

[6]John Yim and Jonathan M Burt. Characterization of vacuum facility background gas through simulation and considerations for electric propulsion ground testing. In *51st AIAA/SAE/ASEE Joint Propulsion Conference*, page 3825, 2015.

[7]Iain D Boyd and Thomas E Schwartzentruber. *Nonequilibrium gas dynamics and molecular simulation*, volume 42. Cambridge University Press, 2017.

[8]Richard E. Wirz, McKenna J. D. Breddan, Mary Konopliv, Patrick Crandall, Graeme Sabiston, Nicolas Rongione, Ehsan Taghizadeh, Richard A. Obenchain, Christopher M. Cretel, Ryan W. Cowan, Luke K. Franz, Blake Haist, Saptarshi Biswas, Mansur Tisaev, and Shehan Parmar. Electric propulsion research activities in the plasma, energy, & space propulsion laboratory. In *38th International Electric Propulsion Conference*, pages IEPC–2024–802, 2024.

[9]T Randolph, V Kim, H Kaufman, K Kozubsky, V Zhurin, and M Day. Facility effects on stationary plasma thruster testing. In *23rd International Electric Propulsion Conference*, pages IEPC–1993–846. The Electric Rocket Propulsion Society Worthington, OH, 1993.

[10]Jason D Frieman, Thomas M Liu, and Mitchell LR Walker. Background flow model of hall thruster neutral ingestion. *Journal of Propulsion and Power*, 33(5):1087–1101, 2017.

[11]Richard A Obenchain and Richard Wirz. Neutral ingestion compensation for gridded ion thrusters via modeling and analysis. In *AIAA SCITECH 2024 Forum*, page 1548, 2024.

[12]John W Dankanich, Mitchell Walker, Michael W Swiatek, and John T Yim. Recommended practice for pressure measurements and calculation of effective pumping speeds during electric propulsion testing. In *Proceedings of the 33rd International Electric Propulsion Conference*, pages IEPC–2013–358, 2013.

[13]Christopher M. Cretel and Richard E. Wirz. Ion thruster grid life and performance prediction via reduced order modeling. In *38th International Electric Propulsion Conference*, pages IEPC–2024–758, 2024.

[14]Chunpei Cai. *Theoretical and numerical studies of plume flows in vacuum chambers*. University of Michigan, 2005.

[15]Jason D Frieman, Thomas M Liu, and Mitchell LR Walker. Background flow model validation with a six-kilowatt hall effect thruster. *Journal of Propulsion and Power*, 36(2):308–311, 2020.

[16]Luke K. Franz and Richarz Wirz. Xe-c scattering, implantation, and sputtering analysis for ep systems. In *38th International Electric Propulsion Conference*, pages IEPC–2024–552, 2024.

[17]Charles Lipscomb, Iain D Boyd, Kaelan B Hansson, Joshua Eckels, and Alex Gorodetsky. Simulation of vacuum chamber pressure distribution with surrogate modeling and uncertainty quantification. In *AIAA SCITECH 2024 Forum*, page 2369, 2024.

[18]Chunpei Cai, Iain D Boyd, and Quanhua Sun. Free molecular background flow in a vacuum chamber equipped with two-sided pumps. *Journal of Vacuum Science & Technology A: Vacuum, Surfaces, and Films*, 24(1):9–19, 2006.

[19]Richard Hofer and Alec Gallimore. Efficiency analysis of a high-specific impulse hall thruster. In *40th AIAA/ASME/SAE/ASEE Joint Propulsion Conference and Exhibit*, page 3602, 2004.

[20]Leanne Liuyue Su, Thomas Marks, and Benjamin A Jorns. Trends in mass utilization of a magnetically shielded hall thruster operating on xenon and krypton. *Plasma Sources Science and Technology*, 2024.

[21]JM Labello, HS Lowry, LM Smith, TM Moeller, and CG Parigger. Modeling of molecular flux in a space simulation chamber. *International Review of Atomic and Molecular Physics*, 2011.

[22]Robert S Martin and Samuel J Araki. Coupling non-maxwellian view factor model to octree based particle vdf compression for accelerated spacecraft-plume simulation. In *36th International Electric Propulsion Conference*, volume 675, pages 2019–733. University of Vienna Austria, 2019.

[23]Samuel J Araki. Radiosity view factor model for sources with general distribution. *Journal of Computational Physics*, 406:109146, 2020.

[24]Samuel J Araki and Robert S Martin. Sputtered atom transport calculation via radiosity view factor model and particle data compression. *Vacuum*, 210:111867, 2023.

[25]GL Saksaganskii. Molecular flow in complex vacuum systems. *CRC Press*, 1988.

[26]Richard E Wirz. *Discharge plasma processes of ring-cusp ion thrusters*. California Institute of Technology, 2005.

[27]Ira Katz and Ioannis G Mikellides. Neutral gas free molecular flow algorithm including ionization and walls for use in plasma simulations. *Journal of Computational Physics*, 230(4):1454–1464, 2011.

[28]David A Brent, Frederick D Cottrell, Kelly A Henderson, and Rudy S Dahbura. Modeling of spacecraft using a modified version of molflux and comparison with a continuous flux model. In *Optical System Contamination V, and Stray Light and System Optimization*, volume 2864, pages 98–106. SPIE, 1996.

[29]Patrick J Roache. Perspective: a method for uniform reporting of grid refinement studies. *Journal of Fluids Engineering*, 1994.

[30]Joint advanced propulsion institute. `https://januselectricpropulsion.com/`. Accessed: 2024-06-20.

[31]Jonathan Walker, Dan Lev, Mitchell LR Walker, Vadim Khayms, and David King. Electrical characteristics of a hall effect thruster body in a vacuum facility testing environment. *Journal of Electric Propulsion*, 1(1):18, 2022.

[32]Richard R Hofer, Sarah E Cusson, Robert B Lobbia, and Alec D Gallimore. The h9 magnetically shielded hall thruster. In *35th International Electric Propulsion Conference*, pages 2017–232. Electric Rocket Propulsion Soc., 2017.

[33]Saptarshi Biswas, Richard A. Obenchain, Ryan W. Cowan, and Richard E. Wirz. Review of pmi data for het-induced erosion of facility surfaces. In *38th International Electric Propulsion Conference*, pages IEPC–2024–532, 2024.

[34]Ryan W. Cowan, Saptarshi Biswas, Luke K. Franz, Christopher M. Cretel, Richard A. Obenchain, and Richard E. Wirz. Hall thruster krypton sputtering effects on vacuum facility materials. In *38th International Electric Propulsion Conference*, pages IEPC–2024–549, 2024.